Journal of Rock Mechanics and Geotechnical Engineering. 2010, 2 (4): 357–364

Journal of Rock Mechanics and Geotechnical Engineering

Journal online: www.rockgeotech.org

# Research on unloading nonlinear mechanical characteristics of jointed rock masses

Jianlin Li[1*], Lehua Wang[1], Xingxia Wang[1, 2], Ruihong Wang[1], Zhuang Cheng[1], Li Dang[1]

[1] *Key Laboratory of Geological Hazards for Three Gorges Reservoir Area of Ministry of Education, China Three Gorges University, Yichang, 443002, China*

[2] *College of Hydraulic and Environmental Engineering, China Three Gorges University, Yichang, 443002, China*

*Received 12 October 2010; received in revised form 5 November 2010; accepted 16 November 2010*

**Abstract:** Geological environments of rock mass projects are always very complicated, and further investigations on rock mechanical characteristics are needed. There are considerable distinctions in rock mechanical characteristics under unloading and loading conditions. A series of tests are conducted to study the stress-strain relationship of rock masses under loading and unloading conditions. Also, the anisotropy, the size effect, and the rheological property of unloading rock mass are investigated. The tests presented in the paper include model test and granite rheological test, which are conducted considering geological condition, rock mass structure, in-situ stress field of the permanent shiplock of the Three Gorges Project. The main differences between loading and unloading rock masses are stress paths, yield criteria, deformation and strength parameters, etc.. Different structural plane directions affect unloading rock mass evidently. With increasing size, the tensile strength, the compressive strength, the deformation modulus, the Poisson's ratio and the anisotropy of rock mass all decrease. For sandstone samples with parallel bedding planes, the cohesion $c$ increases but the internal friction angle $\varphi$ decreases under unloading condition when compared with the values under loading condition. While for samples with vertical bedding planes, the trend is adverse. The rheological property of rocks has close relationship with the tensile stresses of rock masses. When the sandstone samples are tested under high stress condition, their rheological properties are very obvious with the unloading of confining pressure, and three typical rheological stages are shown. Rheological rate changes with the variations in axial stress and confining pressure.

**Key words:** unloading rock mass; unloading test; anisotropy of rock mass; size effect; rheological rate

## 1 Introduction

Theory of unloading rock mass mechanics, a new research field in rock mass mechanics, mainly covers the mechanical properties of unloading rock masses under the actions of gravity, water pressure, seismic loading, etc., as well as its engineering application. It attracts the attention of many scholars [1–17] since the concept of the unloading rock mass mechanics is proposed by Ha et al. [1, 2], and the theory is therein established. Wu et al. [3–8] proposed failure criterion and constitutive relation for unloading rock mass. Wang and Yu [9] studied zoning of slope rock mass after excavation, considering the unloading effect on slope rock mass. Xu et al. [10–13] analyzed the anisotropy, rheological properties of unloading rock mass. Li et al. [14, 15] studied the size effect of unloading rock mass, and Yang et al. [16, 17] focused on deformation properties of unloading rock masses.

In this paper, unloading nonlinear mechanical characteristics (the stress-strain relationship between the anisotropy, the size effect, and the rheological property) of excavated jointed rock mass are studied by a series of tests, including model test based on geological conditions, rock mass structure and the in-situ stress field of the permanent shiplock of the Three Gorges Project, triaxial loading and unloading tests and rheological test of sandstone samples taken from Yichang area.

## 2 Unloading stress-strain relationship of rock mass

### 2.1 Stress-strain relationship of rock mass with unloading model test

Model test is conducted with geological mechanical material. The geological mechanical material is a mixture of the barite powder, iron powder, gypsum and water, considering the actual geological conditions,

Doi: 10.3724/SP.J.1235.2010.00357
*Corresponding author. Tel: +86-13972603868;
E-mail: ljl@ctgu.edu.cn
Supported by the National Natural Science Foundation of China (90610029, 50679079, 50909052)

structural plane of the rock mass and the in-situ stress field of the permanent shiplock of the Three Gorges Project. Experiment with samples whose actual size is 6.75 m × 6.75 m × 6.75 m, in which the geometric similarity ratio $C_L$ is 3, is presented.

The test is performed on a triaxial tester specially designed for unloading experiment of rock masses, whose maximum capacity is 1 500 kN. The components of initial in-situ stress field are $\sigma_x$ (axial direction of the shiplock), $\sigma_y$ (unloading direction) and $\sigma_z$ (vertical direction), and their values are 4, 9 and 3.6 MPa, respectively, according to measurements. First, the loads are applied simultaneously in three directions to the values of actual in-situ stress, and then the sample is unloaded by steps till it fails with tensile stress in *y*-direction based on excavation steps, keeping both $\sigma_y$ and $\sigma_z$ unchanged.

Stress-strain relationship of rock sample in one direction under loading and unloading conditions can be obtained. The curves at unloading can be categorized into 5 sections, as shown in Fig.1. The unloading value at section *oa* is within 30% of the limit unloading capacity, and the deformation at this section is mainly elastic. The unloading value of section *ab* is 30%–80% of the limit unloading capacity, and the deformation at this section is elastoplastic. As for section *bc*, the unloading value is 80%–100% of the limit unloading capacity, and the deformation at this section is mainly plastic. The unloading value of section *cd* exceeds its limit unloading capacity, and the deformation is mainly caused by tension. After point *d*, the stress is above its tensile strength.

Based on the test results, we can see that stress-strain relationships at loading and unloading are different in stress-strain paths, yield conditions, deformations and strength parameters. So mechanical characteristics of rock mass under loading and unloading conditions should be further analyzed and proper stress-strain relationship should be employed during studying practical engineering problems.

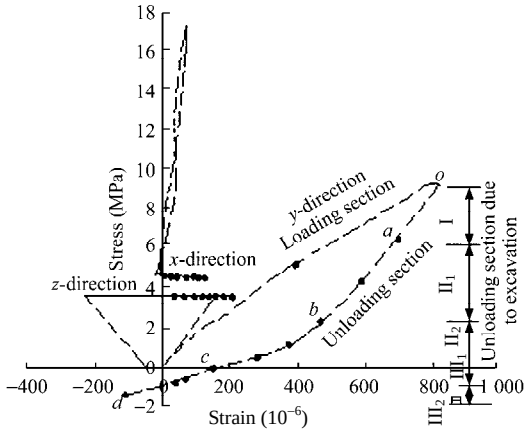


**Fig.1** Stress-strain relationships of unloading rock mass.

### 2.2 Stress-strain relationship of sandstone samples with triaxial unloading tests

The sandstone samples taken from Yichang area are employed in this context. The samples have obvious horizontal bedding by sedimentary, which are intact without appearance of any weathering phenomenon. The samples are cylinders with a diameter of 50 mm and a height of 100 mm, and air-dried. Triaxial unloading tests are conducted on RMT-150C rigid servo-controlled test machine. Tests are performed with three steps:

(1) Gradually apply $\sigma_1 = \sigma_3$ to a preset value (5, 10, 20 and 30 MPa, respectively) at a rate of 0.05 MPa/s. This progress is controlled by stresses.

(2) Maintain $\sigma_3$ as a constant, and raise $\sigma_1$ to a certain value (48%–90% of the peak strength) before the sample failure at a rate of 0.5 MPa/s, in which $\sigma_1$ is larger than the uniaxial compressive strength but smaller than the triaxial compressive strength with corresponding confining pressure. This progress is also controlled by stresses.

(3) Maintain $\sigma_1$ as a constant and gradually reduce $\sigma_3$ at a certain rate (0.1, 0.05 and 0.005 MPa/s, respectively) till the samples are damaged. This progress is controlled by displacements.

The typical unloading stress-strain curves of sandstone samples under the confining pressures of 5, 10, 20 and 30 MPa are shown in Fig.2. The symbols shown in Fig.2 represent sample numbers, axial pressures (MPa) and confining pressures (MPa) at unloading, respectively. The dots on various curves represent the positions when unloading stages begin. The test results are shown in Table 1.

Figure 2 shows that, on the stress-strain curves, there are obviously compression sections in loading

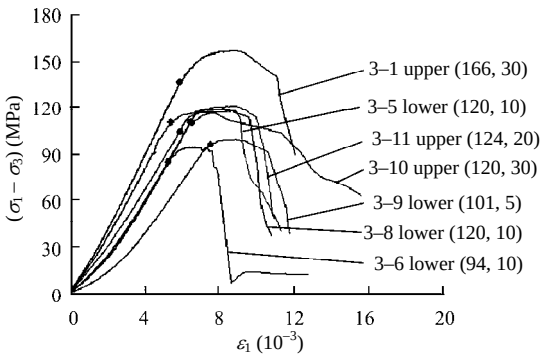


**Fig.2** Unloading stress-strain curves of sandstone samples.

**Table 1** Results of triaxial test of samples at unloading.

| Sample number | Initial confining pressure (MPa) | Axial compressive strength at unloading (MPa) | (Axial pressure /peak strength) (%) | Confining pressure at failure (MPa) | Residual strength (MPa) | Unloading rate (MPa/s) |
|---|---|---|---|---|---|---|
| 3–10 upper | 30 | 120 | 48 | 2.976 | 66.22 | 0.05 |
| 3–1 upper | 30 | 166 | 65 | 9.035 | 99.25 | 0.05 |
| 3–11 upper | 20 | 124 | 65 | 3.413 | 52.59 | 0.05 |
| 3–6 lower | 10 | 94 | 70 | 0.000 | 6.91 | 0.05 |
| 3–5 lower | 10 | 120 | 90 | 2.492 | 43.69 | 0.005 |
| 3–9 lower | 5 | 101 | 80 | 1.185 | 40.12 | 0.05 |
| 3–8 lower | 10 | 120 | 90 | 0.634 | 38.90 | 0.1 |

stage. The curve slopes will increase gradually when the confining pressure increases. When the confining pressure unloads gradually, although $\sigma_1$ remains unchanged, $\varepsilon_1$ increases and there is obviously an axial plastic flow stage. With the gradual increase in $\sigma_1 - \sigma_3$, typical yield stage appears. Comparing with the loading failure, there is no yield stage with increasing confining pressure, and no brittle-ductile transition exists. Whether the confining pressure is high or low, when the samples are damaged due to unloading, the axial strain changes little during peak strength falling to a residual strength with a sudden fracture and ringing sound, showing a very obvious brittle feature; and the stress-strain curves fall sharply. As the test is controlled by stress, the axial pressure drops to a residual strength immediately when the samples are damaged. Compared with the loading failure, unloading failure is more unexpected and severe, yielding more lateral deformations.

The test results are shown in Table 1. We can see that, under the same initial stress, the value of $\sigma_1 - \sigma_3$ for unloading failure is lower than that of axial compressive failure, which demonstrates that rock damage is more easily induced by unloading rather than loading.

# 3 Anisotropy of unloading rock mass

## 3.1 Model test of granite with structural planes in different directions

Thin papers and plastics are used to simulate the structural planes. The length of the structural planes is 3 m, and the connection rate is 50%. Angles between directions of the structural planes and the unloading directions are 8°, 36°, 52°, 82° and 90°, respectively. Unloading stress-strain relationships are obtained and shown in Fig.3, where $\alpha$ is the angle between the direction of the structural plane and the unloading direction, and $R_t$ is the tensile strength.

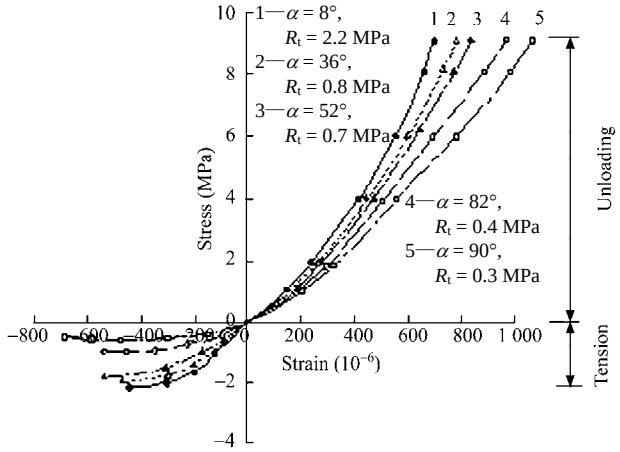


**Fig.3** Stress-strain relationship of unloading rock mass with different structural plane directs.

From Fig.3, it can be seen that, when the angle between the structural plane direction and unloading direction is comparatively small, the slope of stress-strain curve is steep. The curve slope becomes flatter when the angle becomes larger, which shows that structural plane direction greatly affects the unloading curves, as well as the unloading stress-strain curve, the deformation and the strength parameters. Thus, it is deemed that the directions of structural planes affect rock masses at unloading significantly.

## 3.2 Loading and unloading tests of sandstone with structural planes by sedimentary

White sandstone samples are taken from Three Gorges reservoir area with structural planes by sedimentary, whose sizes are $\phi$50 mm × 100 mm. There are 10 samples with parallel bedding planes, and also 10 samples with vertical bedding planes, which are all from the same rock mass, but drilled in different directions, as shown in Fig.4.

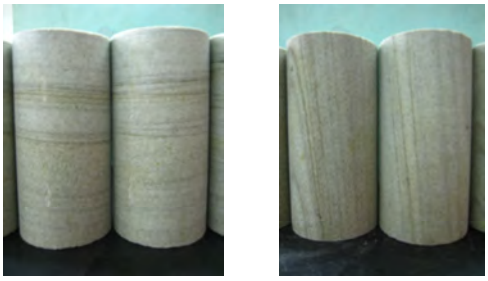

(a) Parallel bedding planes. (b) Vertical bedding planes.

**Fig.4** Sandstone samples with bedding planes in different directions.

In order to ensure the uniform properties of the rock samples, and to obtain better test results, the samples, without any cracks in appearance and with similar rebound values and velocities, are chosen. Rebound

value is one of the evaluation indices of rock mass compressive strength. Rebound values of samples with parallel bedding planes range from 33 to 35, and the longitudinal wave propagation velocities are from 2 222.2 to 2 403.8 m/s. The corresponding values of the samples with vertical bedding planes are 35–38 and 2 617.8–2 793.3 m/s, respectively. The rebound values and velocities of rock samples with parallel bedding planes are comparatively smaller.

3.2.1 *Test schemes*

Schemes I and III are of loading failure modes, while schemes II and IV are of unloading failure modes. In scheme II, axial compression is parallel to bedding planes; while in scheme IV, the axial compression is vertical to bedding planes. Design of test schemes is listed in Table 2.

**Table 2** Design of test schemes.

| Scheme | Failure mode | Initial confining pressure (MPa) |
|---|---|---|
| I | Failure of loading parallel to bedding plane | 5, 10, 15, 20, 25 |
| II | Failure of unloading parallel to bedding plane | 10, 15, 20, 25, 30 |
| III | Failure of loading vertical to bedding plane | 5, 10, 15, 20, 25 |
| IV | Failure of unloading vertical to bedding plane | 10, 15, 20, 25, 30 |

3.2.2 *Test results and analysis*

(1) Anisotropy of loading failure mode

Figure 5 gives the stress-strain curves of loading failure for samples with parallel and vertical bedding planes, respectively, from which the relationship between peak strength and confining pressure can be obtained, as shown in Fig.6.

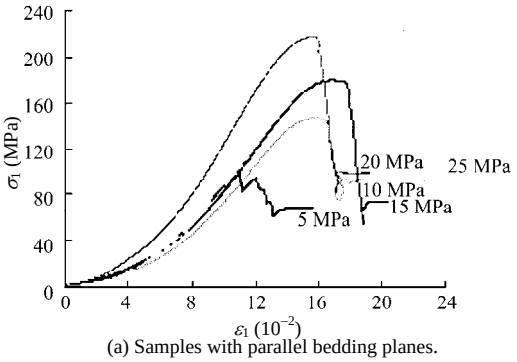


(a) Samples with parallel bedding planes.

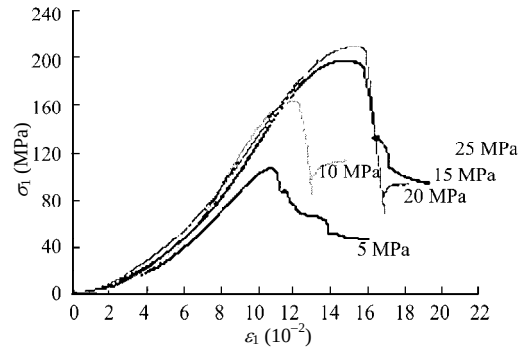


(b) Samples with vertical bedding planes.

**Fig.5** Stress-strain curves of samples with parallel and vertical bedding planes for loading failure mode.

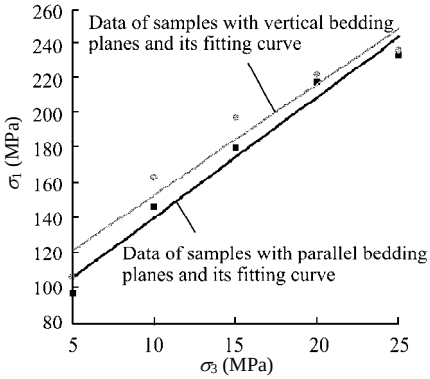


**Fig.6** Relationships between peak strength and confining pressure for loading failure mode.

The relationships between peak strength and confining pressure are approximately linear, and the equations can be obtained by linear regression. The peak strength is the maximum value of $\sigma_1$ when the rock samples are damaged.

For samples with parallel bedding planes, it can be written as

$$\sigma_1 = 72.21 + 6.87\sigma_3 \quad (R^2 = 0.986) \tag{1}$$

For samples with vertical bedding planes, it can be written as

$$\sigma_1 = 101.70 + 5.47\sigma_3 \quad (R^2 = 0.984) \tag{2}$$

where $\sigma_1$ is the peak strength, $\sigma_3$ is the confining pressure, and $R$ is the correlation coefficient.

The strength of samples with vertical bedding planes is always higher under the same confining pressure.

(2) Anisotropy of unloading failure mode

The relationships between peak strength and confining pressure for unloading failure mode are shown in Fig.7. The relationships between peak strength and confining pressure are also linear approximately, and the equations can be obtained by linear regression.

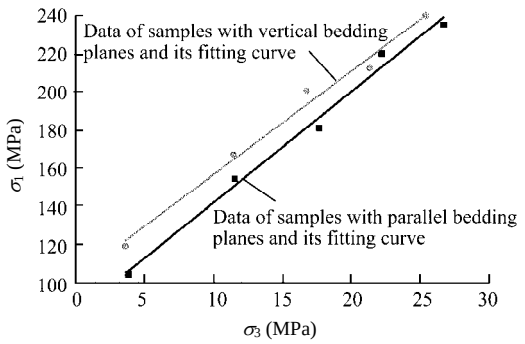


**Fig.7** Relationships between peak strength and confining pressure for unloading failure mode.

For samples with parallel bedding planes, it can be written as

$$\sigma_1 = 82.83 + 5.87\sigma_3 \quad (R^2 = 0.964) \tag{3}$$

For samples with vertical bedding planes, it can be written as

$$\sigma_1 = 90.53 + 6.32\sigma_3 \quad (R^2 = 0.917) \tag{4}$$

The peak strength of samples with vertical bedding planes is higher than that with vertical bedding planes under the same confining pressure and loading or unloading condition.

(3) Shear strength parameters

Test results show that the relationship between peak strength and confining pressure is approximately linear, so Coulomb criterion can be used to explain strength characteristics of sandstone samples. The Coulomb criterion can be modified by $\sigma_1$ and $\sigma_3$:

$$\sigma_1 = Q + K\sigma_3 \tag{5}$$

where $Q$ is equal to the uniaxial compressive strength (actually the uniaxial compressive strength $\sigma_0$ is always smaller than $Q$), and $K$ is influence coefficient of the effect of confining pressures on the triaxial compressive strength.

Relationship between peak strength and confining pressure can be obtained by linear regression, as shown in Eq.(5).

The relationships among the cohesion $c$, internal friction angle $\varphi$ and $Q$, $K$ can be expressed as follows:

$$c = (1 - \sin\varphi)Q / (2\cos\varphi) \tag{6}$$

$$\varphi = \arcsin[(K-1)/(K+1)] \tag{7}$$

Shear strength parameters of the rock masses can be calculated by Eqs.(6) and (7) considering Eq.(5). Parameters for the shear strength of sandstone samples for each test scheme can be obtained by linear regression using Eqs.(5)–(7), and they are listed in Table 3. For samples with parallel bedding planes, the cohesion $c$ increases by 3.3 MPa compared with the values under loading condition, while the internal friction angle $\varphi$ increases by 3.1°. For samples with vertical bedding planes, the cohesion $c$ decreases by 3.7 MPa, but the internal friction angle $\varphi$ increases by 3.1°.

**Table 3** Shear strength parameters for sandstone samples.

| Scheme | $Q$ | $K$ | $c$ (MPa) | $\varphi$ (°) |
|---|---|---|---|---|
| I | 72.21 | 6.87 | 13.8 | 48.2 |
| II | 101.7 | 5.47 | 21.7 | 43.7 |
| III | 82.83 | 5.87 | 17.1 | 45.1 |
| IV | 90.53 | 6.32 | 18.0 | 46.6 |

## 4 Size effect of unloading rock mass

Unloading stress-strain curves of rock mass from permanent shiplock of the Three Gorges Project in different ranges can be obtained by model tests, which can be found in Fig.8. The size of test samples is 250 mm × 250 mm × 250 mm, and the geometric similarity ratios of the test samples are chosen as $C_L$ = 3, 9, 27 and 81 for sample groups A, B, C and D, respectively. Different sample numbers represent various practical ranges. In the tests, the geometric similarity ratio of group A is 3, which represents the size of 0.750 m × 0.750 m × 0.750 m; the geometric similarity ratio of group B is 9, which represents the size of 2.25 m × 2.25 m × 2.25 m; the geometric similarity ratio of group C is 27, which represents the size of 6.75 m × 6.75 m × 6.75 m. The geometric similarity ratio of group D is 81, which represents the size of 20.25 m × 20.25 m × 20.25 m.

Figure 8 shows that the smaller the rock mass size is, the steeper the unloading curve slope is, that is, the smaller the unloading plastic deformation is, the smaller the tensile strain at failure is. Unloading sensitivity of samples with structural planes is enhanced when its size increases, generating more additional plastic deformation and increasing curvature of the unloading curve. Figure 8 also shows that the unloading curves become closer when the simulation range $L$ is larger than 6 m, that is, the size effect of rock mass tends to be stable when the size exceeds a certain value.

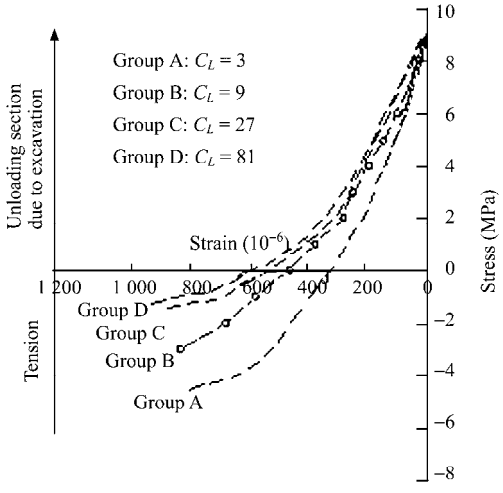


**Fig.8** Unloading curves of sample groups with different geometric similarity ratios.

Structural planes in rock mass increase with increasing size, which leads to a decrease in rock mass strength. Table 4 shows that all rock mass moduli decrease obviously when the size increases. Compressive deformation modulus becomes stable when $C_L$ = 27 ($L$ > 6.75 m), and the initial deformation modulus is the same while tensile deformation

**Table 4** Variations in modulus of deformation and size of rock.

| Size (m × m × m ) | Compressive deformation modulus (GPa) | Tensile deformation modulus (GPa) | Initial unloading deformation modulus (GPa) |
|---|---|---|---|
| 0.75 × 0.75 × 0.75 | 50 | 6 | 35 |
| 2.25 × 2.25 × 2.25 | 45 | 4 | 32 |
| 6.75 × 6.75 × 6.75 | 38 | 2 | 28 |
| 20.25 × 20.25 × 20.25 | 35 | 1.5 | 26 |

modulus is a little more sensitive to rock size, which is also stable when $C_L$ = 81 ($L$ = 20.25 m). So results of $C_L$ = 81 should be employed during calculating rock mass deformation modulus.

When $C_L$ = 27 ($L$ > 6.75 m), the compressive strength, which is already stable, is about 60% of the ultimate bearing capacity of rock mass without structural planes, and the variation in tensile strength becomes stable gradually. When $C_L$ > 81 ($L$ > 20.25 m), the tensile strength is stable at 1.3 MPa.

It can be found that the larger the size is, the larger the Poisson's ratio is, but the Poisson's ratio is very small for samples without cracks, and it increases rapidly for samples with cracks. Rock mass size also has effects on the Poisson's ratio, and it becomes stable when the size reaches a certain range/value under loading or unloading condition.

# 5 Rheological characteristics of unloading rock mass

### 5.1 Tensile rheological test for granite samples

Tensile and tensile-shear rheological tests are conducted using rock cores taken from the permanent shiplock of the Three Gorges Project. The rock samples are granite, 54 mm in diameter, and 200 or 150 mm in length. Values of tensile stress ratio $\beta$ ($\beta$ is the ratio of preset tensile stress to failure stress) are 0.3, 0.4, 0.5, 0.6, 0.7, 0.8, 0.9 and 1.0, respectively. These six kinds of rheological relationship curves are shown in Fig.9, and the test results are shown in Table 5.

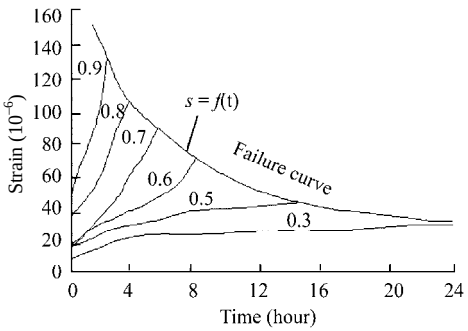


**Fig.9** Rock rheological relationship curves.

**Table 5** Rheological durations and limit tensile strains of granite samples under different tensile stress ratios.

| Tensile stress ratio($\beta$) | Limit tensile strain ($10^{-6}$) | Rheologic duration |
|---|---|---|
| 0.3 | – | > 6 months |
| 0.4 | – | > 6 months |
| 0.5 | 40 | 14.5 hours |
| 0.6 | 65 | 6.5 hours |
| 0.7 | 78 | 4.5 hours |
| 0.8 | 105 | 3.0 hours |
| 0.9 | 136 | 2.0 hours |
| 1.0 | 150 | ≈0 |

Figure 9 shows that tensile rheology of the rock mass develops swiftly when the tensile stress ratio $\beta$ is not less than 0.5 ($\beta \geq 0.5$). The larger the tensile stress ratio is, the shorter the rheological duration is. More quickly, it develops and fails, which demonstrates that the tensile rheology under high stress develops faster, revealing the property of brittle rupture. When $\beta < 0.5$, the rheology of the test samples is significant, and it lasts for a long period of time. Taking $\beta$ = 0.3 as an example, the rheological deformation of the test samples lasts for more than six months (these samples are not damaged after six months' observation), which illustrates that rock masses at a low stress shows an significant tensile rheology. Consequently, rock mass tensile rheological properties are directly related to the tension on it. Brittle rupture occurs when rock mass is under tension. Fitting the points when the samples are broken under all tensile stress ratios can get the failure curves (horizontal and vertical coordinates show rheological duration coordinate and the limit tensile strain of the rock, respectively, when the rock sample is damaged).

### 5.2 Rheological test of sandstone samples under unloading condition

Rheological test is conducted in a manner of hierarchical unloading. The sandstone samples are cylinders with the size of $\phi$50 mm × 100 mm. The test is conducted by the following three steps:

(1) Increase the hydrostatic pressure to 30 MPa at a rate of 0.05 MPa/s.

(2) Maintain the confining pressure of 30 MPa, and gradually apply the axial force till a preset value at a rate of 0.5 kN/s and remain the axial stress unchanged for hours after the stabilization of the deformation.

(3) Maintain the axial pressure $\sigma_1$ constant and gradually unload the confining pressure by 5 MPa at each step after the rheological deformation of the rock samples is stable under the former load level.

The rheological test curves of unloading confining pressures for the sandstone samples at $\sigma_1$ = 100, 135 and 185 MPa, are given in Fig.10. It can be found

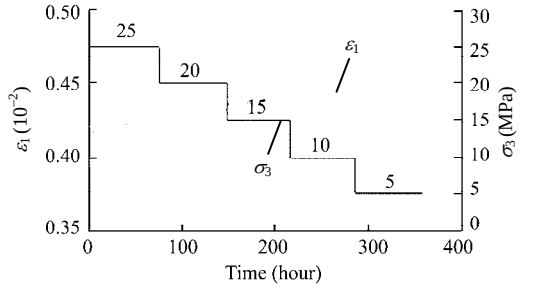


(a) $\sigma_1$ = 100 MPa.

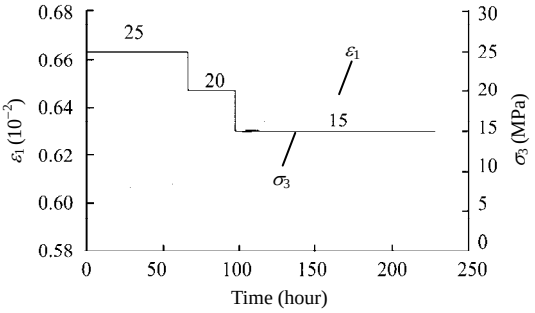


(b) $\sigma_1$ = 135 MPa.

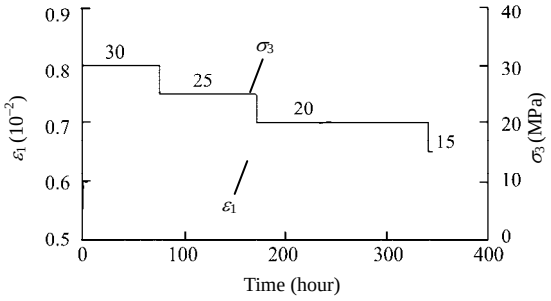


(c) $\sigma_1$ = 185 MPa.

**Fig.10** Rheological curves with different unloading confining pressures.

that obvious rheological phenomena occur as a result of the long-term external load. When unloading the confining pressure step by step, and remaining the stress and confining pressures unchanged, the rheological deformation property becomes much obvious. Rheology of sandstone samples shows that three typical stages can be regarded, that is, primary attenuation rheological stage, steady rheological stage and accelerative rheological stage, before a nonlinear accelerative rheological failure. Samples under lower stress and higher confining pressure have less rheological deformation. The rheological curves can be fluctuant, but the overall trend is stable.

The complete rheological curve under the confining pressure of 15 MPa and the stress level of 135 MPa is shown in Fig.11, where three stages of the rock rheology are included. The duration and deformation of the primary attenuation rheological stage and the

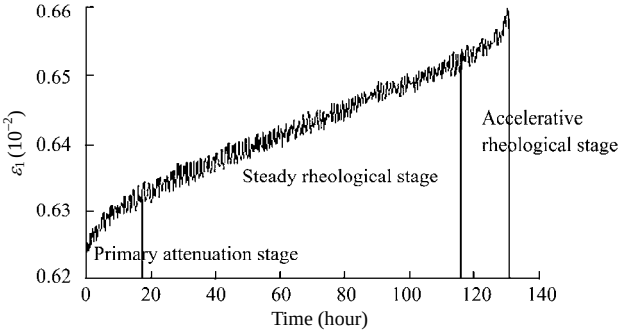


**Fig.11** Complete rheological curve of sandstone samples.

accelerative rheological stage are smaller compared with the steady rheological stage, which occupies most of the complete curve and over 70% of the duration of accelerative rheological stage; while the primary attenuation rheological stage and nonlinear accelerative rheological stage both occupy a small amount of the complete rheological curve. The deformation of steady rheological stage under long-term constant external force is dominant in the whole rheological stage, above 50% of the whole deformation of the rheological stage.

Figure 12 shows that the rheological rate of primary attenuation rheological stage becomes smaller gradually, from $7.9 \times 10^{-2}$ to $0.5 \times 10^{-2}$ mm/d, and then it becomes stable eventually. The average rheological rate in primary attenuation rheological stage is about $1.6 \times 10^{-2}$ mm/d. At the steady rheological stage, the rheological rate remains unchanged with a value about $0.5 \times 10^{-2}$ mm/d. Before entering accelerative deformation stage, the rheological rate increases rapidly from $0.5 \times 10^{-2}$ to $12.1 \times 10^{-2}$ mm/d, and at this time, the samples are damaged. In general, the average rheological rate in a nonlinear accelerative rheological stage is $1.2 \times 10^{-2}$ mm/d.

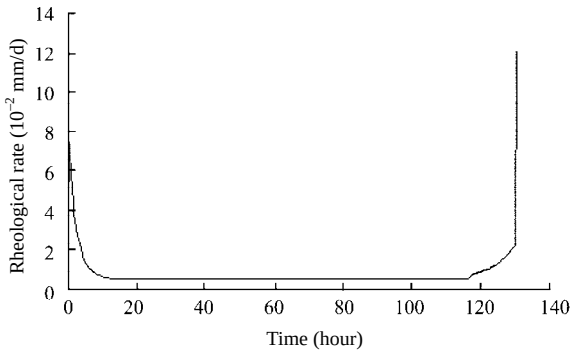


**Fig.12** Rheological rate curve of three rheological stages for sandstone samples.

We can conclude from above-mentioned results that the rheological property of sandstone samples under unloading condition is evident, and the rheological

deformation is large. The steady rheological stage is dominant, while primary and nonlinear accelerative rheological stages are the secondary. The rheological rate first decreases to a certain value, and then keeps constant, and finally increases nonlinearly.

# 6 Conclusions

In this paper, we study the unloading nonlinear mechanical characteristics of excavated rock mass by a series of tests. Some useful conclusions can be drawn from the test results:

(1) Stress-strain relationships of rock masses are different in stress-strain paths, yield conditions, parameters and analysis methods under loading and unloading conditions.

(2) Different structural plane directions affect rock mass property at unloading evidently.

(3) For sandstone samples with structural planes by sedimentary, the relationship between the peak strength and the confining pressure is approximately linear. The strength of samples with vertical bedding planes is larger than that of samples with parallel bedding planes. For samples with parallel bedding planes, the cohesion $c$ increases but the internal friction angle $\varphi$ decreases under unloading condition, compared with the values under loading condition. For samples with vertical bedding planes, the trend is adverse.

(4) The stress-strain relationship, compressive strength, tensile strength, deformation modulus, Poisson's ratio and anisotropy of the rock mass vary with the sizes of samples. When the size of granite samples is larger than 6.75 m ($C_L$ = 27), the size effect, the compressive strength, the compressive deformation modulus, the initial unloading deformation modulus and the Poisson's ratio will be stabilized basically. While in terms of the tensile strength, tensile deformation modulus, the size effect will be stabilized only when the size of the rock mass is larger than 20.25 m ($C_L$ = 81).

(5) Rheological property has a close relationship with the magnitude of rock mass tensile stress. Rock mass with a lower stress shows a more significant tensile rheology.

(6) When stress level is low and confining pressure is high, the rheological deformation of sandstone samples is not obvious. When the tests on sandstone samples are conducted under high stress level, its rheological property is evident with confining pressure unloading, showing three typical rheological stages.

(7) Rheological rate changes with the variations in stress level and confining pressure, which includes two stages when confining pressure is high. With the decreasing of confining pressure, the rheological rate first decreases to a certain value, and then keeps constant, and finally increases nonlinearly.

## References

[1] Ha Qiuling. Rock slope engineering and unloading nonlinear rock mass mechanics. Chinese Journal of Rock Mechanics and Engineering, 1997, 16 (4): 386–391 (in Chinese).

[2] Ha Qiuling, Li Jianlin. Study of macroscopic mechanics parameters for the unloading rock mass of rock slope. Beijing: China Architecture and Building Press, 1996 (in Chinese).

[3] Wu Gang. Experimental investigation on unloading failure of intact rock mass model. Journal of Experimental Mechanics, 1997, 12 (4): 459–555 (in Chinese).

[4] Li Jianlin. Failure criterion and its parameters of rock mass triaxial strength. Journal of University of Hydraulic and Electric Engineering (Yichang), 1998, 20 (2): 1–5 (in Chinese).

[5] Zhang Qiangyong, Zhu Weishen, Chen Weizhong. Analysis of elastoplastic damage for high jointed slope of the Three Gorges Project shiplock during unloading due to excavation. Journal of Hydraulic Engineering, 1998, (8): 20–22 (in Chinese).

[6] Ha Qiuling, Li Jianlin, Zhang Yongxin, et al. Nonlinear mechanics of jointed rock during unloading. Beijing: China Architecture and Building Press, 1998 (in Chinese).

[7] Li Jianlin. Theory and application of unloading rock mass. Beijing: China Architecture and Building Press, 1999 (in Chinese).

[8] Ha Qiuling. Simulation analysis of rock mass engineering and rock mass mechanics—a study of anisotropic excavation unloading rock mass mechanics. Chinese Journal of Geotechnical Engineering, 2001, 23 (6): 664–668 (in Chinese).

[9] Wang Junhuai, Yu Yongzhi. Rock deformation of unloaded loose zone of high excavated slope at TGP's shiplock. Yangtze River, 1999, 30 (4): 4–6 (in Chinese).

[10] Xu Ping, Zhou Huoming. Rheological analysis of rock mass of high slope considering effects of excavation unloading. Chinese Journal of Rock Mechanics and Engineering, 2000, 19 (4): 481–485 (in Chinese).

[11] Li Jianlin, Meng Qingyi. Anisotropic study of unloaded rock mass. Chinese Journal of Rock Mechanics and Engineering, 2001, 20 (3): 338–341 (in Chinese).

[12] Li Jianlin, Xiong Junhua, Yang Xuetang. Experimental investigation on unloading mechanical characteristic of rock mass. Water Resources and Hydropower Engineering, 2001, 32 (5): 48–51 (in Chinese).

[13] Zhou Weiyuan, Yang Ruoqiong, Yan Gongrui. Nonlinear and discontinuous deformation and rheological analysis of unloaded rock slopes. Chinese Journal of Rock Mechanics and Engineering, 1997, 16 (3): 210–216 (in Chinese).

[14] Li Jianlin, Wang Lehua. Study on size effect of unloaded rock mass. Chinese Journal of Rock Mechanics and Engineering, 2003, 22 (12): 2 032–2 036 (in Chinese).

[15] Li Jianlin. Unloading rock mass mechanics. Beijing: China Water Power Press, 2003 (in Chinese).

[16] Yang Xuetang, Ha Qiuling, Gao Xizhang, et al. Research on unloading deformation and support of high slope of thick soft rock interlaced with hard rock. Chinese Journal of Rock Mechanics and Engineering, 2004, 23 (16): 2 681–2 686 (in Chinese).

[17] Sheng Junhui, Wang Lansheng, Wang Qinghai, et al. Deformation and fracture features of unloaded rock mass. Chinese Journal of Rock Mechanics and Engineering, 2003, 22 (12): 2 028–2 031 (in Chinese).